10-2023

Development of Prediction Method for Dimensional Stability of 3D-Printed Objects

Kyung-Eun Min
Portland State University

Jae-Won Jang
Portland State University

Jesik Shin
Korea Institute of Industrial Technology

Cheolhee Kim
Portland State University, cheol@pdx.edu

Sung Yi
Portland State University

Citation Details

Min, K. E., Jang, J. W., Shin, J., Kim, C., & Yi, S. (2023). Development of Prediction Method for Dimensional Stability of 3D-Printed Objects. Applied Sciences, 13(19), 11027.

applied sciences

MDPI

Article

Development of Prediction Method for Dimensional Stability of 3D-Printed Objects

Kyung-Eun Min [1], Jae-Won Jang [1], Jesik Shin [2], Cheolhee Kim [1,2,*] and Sung Yi [1,*]

[1] Department of Mechanical and Material Engineering, Portland State University, Portland, OR 97201, USA; min3@pdx.edu (K.-E.M.); jaewon@pdx.edu (J.-W.J.)
[2] Welding and Joining R&D Group, Korea Institute of Industrial Technology, 156 Getbeol-ro, Yeonsu-gu, Incheon 21999, Republic of Korea; jsshin@kitech.re.kr
* Correspondence: cheol@pdx.edu (C.K.); syi@pdx.edu (S.Y.)

Abstract: Fused deposition modeling (FDM), as one of the additive manufacturing processes, is known for strong layer adhesion suitable for prototypes and end-use items. This study used a multiple regression model and statistical analysis to explore the dimensional accuracy of FDM objects. Factors such as inclination angle, layer thickness, support space, and raster angle were examined. Machine learning models (Gaussian process regression (GPR), support vector machines (SVM), and artificial neural network (ANN)) predicted dimensions using 81 datapoints. The mean squared dimensional error (MSDE) between the measured and designed surface profiles was selected as an output for the dimensional accuracy. Support spacing, layer thickness, and raster angle were determined to be statistically significant, and all factors were confirmed as significant predictors. The coefficients of determination for multiple linear regression, GPR, SVM, and ANN models were 76%, 98%, 93%, and 99%, respectively. The mean absolute errors (MAEs)—errors between the measured and the predicted MSDEs—were 0.020 mm and 0.034 mm, respectively, for GPR and SVM models. The MAEs for ANN models were 0.0055 mm for supporting cases and 2.1468×10^{-5} mm for non-supporting cases.

Keywords: fused deposition modeling; multiple regression model; ANOVA; artificial neural network

Citation: Min, K.-E.; Jang, J.-W.; Shin, J.; Kim, C.; Yi, S. Development of Prediction Method for Dimensional Stability of 3D-Printed Objects. *Appl. Sci.* **2023**, *13*, 11027. https://doi.org/10.3390/app131911027

Academic Editor: Soshu Kirihara

Received: 12 September 2023
Revised: 28 September 2023
Accepted: 3 October 2023
Published: 6 October 2023

1. Introduction

Additive manufacturing (AM) systems have undergone rapid advancements in recent decades, garnering significant research interest and widespread media attention. AM technology has demonstrated immense potential in the production of highly valuable and intricate products and parts. This manufacturing process involves the layer-by-layer addition of materials, utilizing the geometry directly obtained from computer-aided design (CAD) models [1–3]. The ability to create customized and complex objects through additive manufacturing opens up new opportunities for the manufacturing industry, enabling the production of individually tailored products with enhanced functionality and design [4–6]. In recent times, there has been notable progress in the utilization and advancement of various AM processes, encompassing a wide range of techniques and materials, with a particular focus on polymers [7]. Moreover, the extensive range of applications offered by additive manufacturing plays a pivotal role in driving the remarkable growth of the associated market. This is attributed to the capability of additive manufacturing to cater to diverse sectors within the manufacturing industry, including household electrical appliances, aerospace, automotive, sportswear, bio/medical devices, integrated circuit boards, the food industry, etc. [8–14].

AM processes widely used are material jetting, vat photopolymerization, powder bed fusion, material and binder jetting, and material extrusion. The material jetting process uses the multijet printing (MJP) technique that uses piezo printhead technology to deposit materials layer by layer. MJP is resin-based 3D printing, and UV-curable resins and waxes, such as acrylates, epoxies, polylactide, polycaprolactone, etc., are used in the MJP

technique. The vat photopolymerization process uses stereolithography (SLA) and digital light processing (DLP). SLA uses a UV radiation beam to solidify photo resin layers on a vat of liquid resin. DLP uses light projectors below the resin and projects an entire layer at a time using an array of micrometer-sized mirrors. SLA and DLP are resin-based 3D printings as well, and UV-curable resins, waxes, and resins with photo-active monomers, such as ABS, acrylics, epoxides, polycaprolactone, poly lactic-co-glycolic acid, etc., are used. The power bed fusion process applies the selective laser sintering (SLS) technique that uses a laser beam or sintering to solidify polymer powder particles layer by layer. Compacted fine powders or thermoplastics materials, such as nylon, polycaprolactone, polyvinyl alcohol, polylactide, etc., are used. The material extrusion process uses the fused deposition modeling (FDM) method, and a molten material via a nozzle, such as a polymer, is deposited layer by layer to create a 3D product. Thermoplastics and polymers, such as ABS, polylactic acid (PLA), polycaprolactone (PCL), polyethylene, nylon, etc., are used [4,5,8,15].

FDM technology is a representative technique of material extrusion. It melts thermoplastics and extrudes melted material via a nozzle. FDM is becoming more attractive for 3D printing with increasing applicable material in various fields. FDM parts exhibit good layer adhesion and strength, making them suitable for functional prototypes and end-use parts. The technology also offers design flexibility, allowing for the creation of complex geometries and the integration of features like threads and hinges. Additionally, FDM is known for its speed in producing larger parts. Along with the increase in the use of FDM, the result prediction, such as dimensional accuracy and surface quality, is also gaining a lot of attention. FDM can easily be applied for all of these; however, predicting the printing result is one of the main challenges in FDM because the printing parameters and the conditions are enormous. For example, various printing parameters, such as inclination angle, layer thickness, support spacing, and raster angle, should be considered before printing as well as printing conditions like printing temperature, printing speed, and fill density [4,5,8,16,17].

Researchers have introduced and released the dimensional accuracy of parts based on polymer materials extracted using FDM. Chang and Huang [18] investigated the accuracy of an FDM model with various elements of transmission machinery and differing filament diameter. Therefore, they considered profile error and extruding apertures as two substantial quality factors. An original image measurement method for investigating profile error using a series of standard cylinders laid on the contour of the part was proposed, and the effects of extruding apertures on model accuracies, such as contour width, contour depth, part raster width, and raster angle, were analyzed using the Taguchi method. From the results, the contour width is the important factor affecting profile error and aperture area. Saqid and Urbanic [19] studied the impact of geometric forms along with process parameters on part accuracy for the FDM process. A general factorial design, with simple geometric shapes, including thick-wall and thin-wall features, was developed, and three response variables (perpendicularity, cylindricity, and flatness) were measured to investigate accuracy. The effects of process parameters, such as the position of the part in the work envelope, layer thickness, and orientation of the test models, were investigated. They proposed that the geometry and feature interfaces affected the accuracy more than the process parameter. Akbas et al. [20] investigated the effect of the nozzle temperature and feed rates on the dimensions of an FDM part made of ABS and PLA experimentally and numerically. An increase in the feed rate resulted in a reduction in strip width. Furthermore, when evaluating the effect of nozzle temperature and feed rate on strip width, it was found that the measurement positions had a more significant influence. The numerical model accurately predicted the experimental data, exhibiting a high level of agreement. However, some disparities were noted at elevated feed rates and nozzle temperatures. Park et al. [21] investigated the dimensional accuracy and surface characteristics of different areas in 3D-printed dental casts made with various 3D printing methods. From the superimposing analysis, it was observed that FDM exhibited more systematic deviations compared to DLP,

PolyJet, and SLA techniques. The three-dimensional deviations at each cylinder location were found to be the lowest in the left canine region, and deviations increased as the distance from this specific site increased in all the studied groups.

Machine learning technology has experienced notable progress in recent years, primarily attributed to the availability of extensive datasets, enhanced computational capabilities, and refined algorithms. Machine learning offers several advantages such as its proficiency in handling voluminous and intricate datasets, its capability to automate decision-making processes, its ability to identify intricate patterns or anomalies that may pose difficulties for humans, and its potential to enhance predictive accuracy and generate valuable insights over time [22,23]. Consequently, machine learning has the potential to augment efficiency, precision, and innovation within numerous industries. Nonetheless, the field also presents challenges concerning the quality of data, potential biases within datasets or algorithms, the interpretability of complex models, and ethical considerations [24,25].

Various prediction and optimization studies related to a machine learning model have been released. Min et al. [26] predicted and optimized the shear strength and curing time of non-conductive adhesives (NCAs) using an artificial neural network (ANN) model. The model accuracy was improved by 28.9–35.2% compared to other studies. They proposed the optimized NCA formulation as the range of 0.2137 × (resin content in phr) + (catalyst content in phr) $\geq$ 35.87 for mass production requirements. Sood et al. [27] studied the statistical analysis of the dimensional accuracy in the FDM process using parameters such as layer thickness, part orientation, raster angle, air gap, and raster width. To optimize the percentage change in length, width, and thickness simultaneously, the grey Taguchi method is employed to determine the optimal levels of process parameters. In addition, they predicted overall dimensional accuracy using the ANN model. The errors between predicted data and measured data were 0–3.5%. Mohamed et al. [28] investigated the effects of FDM fabrication conditions on dimensional accuracy. An ANN model was employed to predict and optimize the effects of six operating parameters including slice thickness, raster air gap, deposition angle, print direction, width, and perimeters. The R^2 was over 99%, and the minimum percentage differences in length (0.244 mm, 4%) and diameter (0.480 mm, 3%) were obtained.

Recently, studies based on the prediction and optimization of experimental parameters for additive manufacturing have emerged. However, the FDM process is characterized by its high complexity, and there is a scarcity of theoretical models available for the purpose of prediction. The complexity of the printed 3D object has a detrimental effect on its accuracy, resulting in decreased levels of precision. From a review of the literature, it can be seen that some AM processes have limitations for comprehensive mathematical models, making it difficult to predict and optimize parameters accurately. AM parameter optimization often involves multiple interdependent variables. Optimizing across numerous variables can be challenging and may lead to suboptimal solutions. Moreover, the accuracies of the objects—including support bars and inclination angle—preventing the reflection of the object, were not studied. In this paper, 3D objects were printed with various support bars and inclination angles through the FDM process, and the quality of the 3D-printed object were evaluated. First, primary factors were analyzed for the improvement of the printing quality through the multiple regression model and analysis of variance. Second, prediction machine learning models were developed for predicting printing accuracy. From the results, the prediction models for the dimensional accuracies of FDM 3D-printed objects were developed.

2. Experiments

2.1. Materials and 3D Printing

In this study, PLA was employed as the material for FDM 3D printing. Filament-type PLA was provided by Polymaker (Shanghai, China) and was used for 3D printing, and the filament diameter was 2.85 mm. The material properties are listed in Table 1.

Table 1. Material properties.

Material	Density (g/cm^3 at 21.5 °C)	Glass Transition Temp. (°C)	Melting Temp. (°C)	Young's Modulus (MPa)	Tensile Strength (MPa)	Tensile Strength (MPa)
PLA	1.17–1.24	61	150	2636 ± 330	46.6 ± 0.9 (XY axis)	43.5 ± 3.1 (Z axis)

The FDM 3D printing equipment was Ultimaker 2+ (Ultimaker, Utrecht, The Netherlands) with the principal specifications detailed in Table 2. The design of three-dimensional models for 3D printing was executed using Solidworks 2021 (SolidWorks Corp., Dassault Systèmes, Waltham, MA, USA). Subsequently, the designed 3D model was saved in the standard triangle language (STL) file format. Each model was sliced by Ultimaker Cura 5.0.0 (Ultimaker, Utrecht, The Netherlands), and G-code was generated.

Table 2. Specifications of FDM 3D printing equipment.

Model	Ultimaker 2+ (Ultimaker, The Netherlands)
Build volume (mm)	223 × 220 × 205
Layer resolution (μm) @ 0.4 mm nozzle	20–200
Accuracy (μm)	12.5 in XY axis 5.0 in Z axis

The base model dimensions encompass 10 mm × 10 mm × 25 mm along the XYZ axis. Variable printing parameters included the inclination angle, layer thickness, support spacing, and raster angle (Table 3). An illustrative model design is presented in Figure 1. The models featuring inclination angles of 60° and 75° were printed without the application of support structures.

Table 3. Design parameters.

Factors	Level				
	1	2	3	4	5
Inclination angle (°)	15	30	45	60	75
Layer thickness (mm)	0.2	0.4	0.6	-	-
Support space (mm)	5	10	15	-	-
Raster angle (°)	0	45	90	-	-

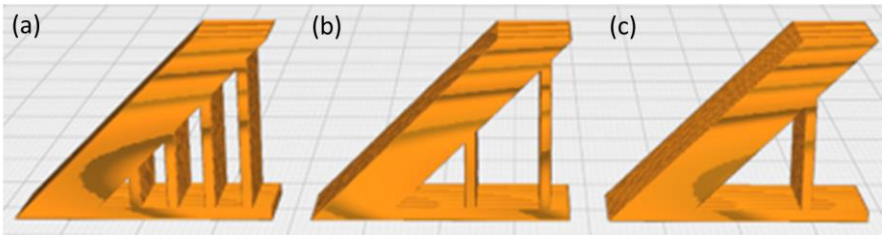

Figure 1. Designed 3D object with 45° inclination angle and support space of (**a**) 5 mm, (**b**) 10 mm, and (**c**) 15 mm.

For comparison of the variable parameters, additional printing conditions including printing temperature, nozzle movement speed, and infill density were held constant (Table 4). Subsequent to printing, all 3D objects were subjected to a 3 h cooling period.

Table 4. Printing conditions.

Material	PLA
Nozzle temperature (°C)	210
Bed temperature (°C)	60
Nozzle moving speed (mm/s)	60
Infill density (%)	100

2.2. Measurement of the Printed Object

The surface profile of the 3D object printed by the FDM process was measured by the optical measurement inspection system. The measuring equipment was Datastar 200 from RAM Optical Instrumentation Incorporated (Rochester, NY, USA) with the main specifications detailed in Table 5.

Table 5. Specifications of RAM optical measurement inspection system.

Model	Datastar 200 (RAM Optical Instrumentation Incorporated, Rochester, NY, USA)
Measuring range (mm)	200 × 150 × 150
Optical magnification	×35–×280
Resolution (μm)	0.5
Max. measured load (kg)	23
Accuracy (μm)	2.5 in XY axis 5.0 in Z axis

The base, slope, and top lines of the side surfaces of the objects were inspected to investigate the dimensional accuracy between measured and designed profiles, and the edges of the side surface were subjected to scanning. The base line of the measured surface profile was considered as the parallel line along the *X*-axis, meaning that it was assumed to match the designed base line of the 3D object; then, the slope and top lines were utilized for dimensional accuracy analysis (Figure 2). The mean squared dimensional error (MSDE) between measured and designed profiles in the slope and top lines was calculated and was denoted as a representative output for the dimensional accuracy of this study.

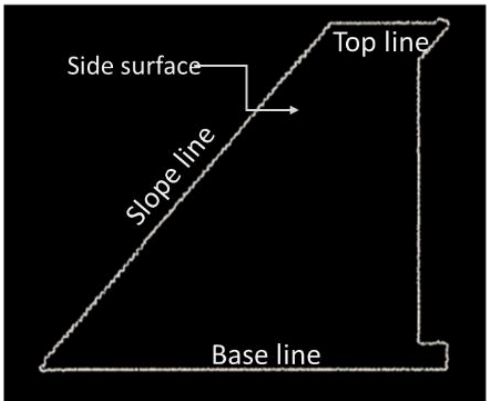

Figure 2. Measured profile of the object.

2.3. Regression Models

In this study, three types of regression models were employed to predict 3D object dimensions. A multiple linear regression model was employed for the analysis, while Gaussian process regression (GPR) and support vector machines (SVM) algorithms were implemented using MATLAB version R2021a. Additionally, an ANN model was constructed using Python for the purposes of comparison and evaluation.

The input parameters were inclination angle, layer thickness, support space, and raster angle, and the output parameters were the MDSEs for dimensional accuracies of the objects. A total of 81 datapoints were used for the prediction of 3D objects. These 81 datapoints were randomly divided into training, validation, and test datasets at a ratio of 70%, 15%, and 15%, respectively.

ANN model was employed with three hidden layers and 32 nodes. A rectified linear unit (ReLU) activation function was used. The mean absolute errors (MAEs) loss function and adaptive moment estimation (ADAM) optimizer, including a learning rate of 0.001, $\beta 1 = 0.9$, $\beta 2 = 0.999$, and $\varepsilon = 10^{-8}$, were applied in model training and optimization. The models were trained for 200 epochs with minibatches of 10 to avoid the overfitting issue. The flow chart for ANN model is shown in Figure 3.

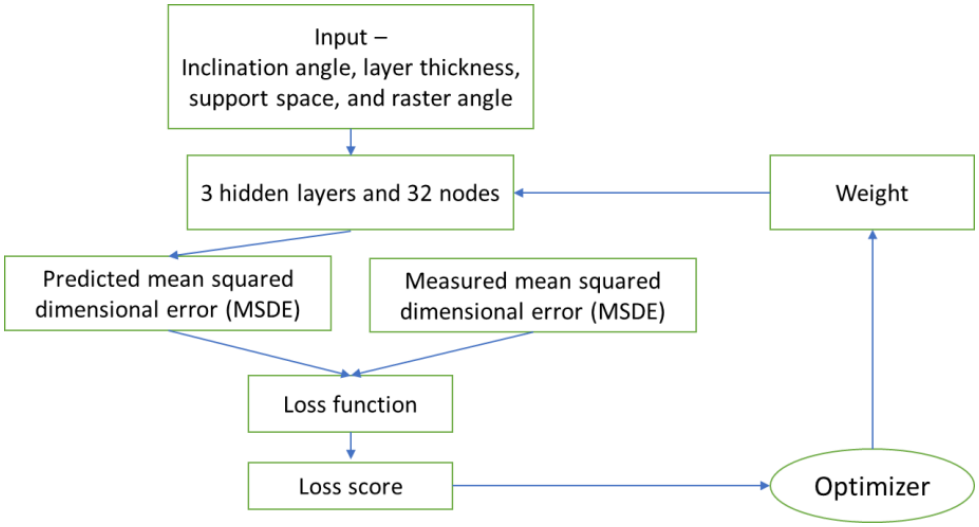

Figure 3. The flow chart for ANN model.

3. Results

3.1. Stacking Profiles

All designed 3D objects were printed three times to assess the stacking profile, which was defined as the outline of the printed object in the XZ plane. The printed objects formed a rectangular bar without noticeable flaw (Figure 4a). The printed 3D objects, with a 45° inclination angle and support spaces of 5, 10, and 15 mm, are shown in Figure 4b.

Figure 4. Printed 3D objects of (**a**) all objects and (**b**) with 45° inclination angle and support spaces of 5 mm, 10 mm, and 15 mm.

The stacking profiles were used to evaluate the dimensional accuracy compared to the original design. Measured profiles were expressed in red lines and compared to the designed profiles in black lines (Figure 5). The differences between measured and designed profiles were recorded and set as output for the dataset.

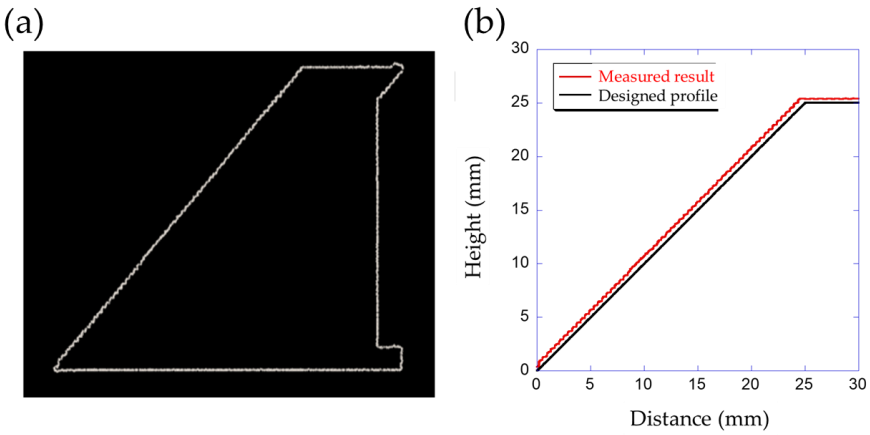

Figure 5. Stacking profiles: (**a**) measured stacking profile and (**b**) comparing measured and designed profiles.

3.2. Correlation Analysis

Tables 6 and 7 show the correlation coefficients between process parameters and the MSDE (output) for supporting cases and non-supporting cases, respectively. As shown in Table 6, Pearson correlation coefficients for support spacing, layer thickness, raster angle, and inclination angle were −0.436, 0.565, 0.477, and −0.152, respectively. *p*-values were 0 for supporting spacing, layer thickness, and raster angle and 0.177 for inclination angle. As shown in Table 7, Pearson correlation coefficients for layer thickness, raster angle, and inclination angle were 0.754, −0.254, and 0.157, respectively. *p*-values for layer thickness, raster angle, and inclination angle were 0, 0.308, and 0.534, respectively.

Table 6. The correlation coefficient for supporting cases.

	Supporting Spacing	Layer Thickness	Raster Angle	Inclination Angle
Pearson, R	**−0.436**	**0.565**	**0.477**	−0.152
p-value	**0.0**	**0.0**	**0.0**	0.177

Table 7. The correlation coefficient for non-supporting cases.

	Layer Thickness	Raster Angle	Inclination Angle
Pearson, R	**0.754**	−0.254	0.157
p-value	**0.0**	0.308	0.534

In cases where support was utilized, the influences of support spacing, layer thickness, and raster angle were found to be statistically significant relationships with the dependent variable, as indicated by a *p*-value below 0.05. By the Pearson correlation coefficients, support spacing exhibited a negative relationship, while layer thickness and raster angle indicated positive relationships, and layer thickness exhibited the most prominent degree of correlation. In cases where support was not utilized, only layer thickness exhibited statistically significant influence, as evidenced by *p*-values below 0.05 and the highest positive level of correlation.

3.3. Multiple Linear Regression Model Analysis

The multiple linear regression model was employed to investigate the relationships between the parameters (support spacing, layer thickness, raster angle, and inclination angle) and the MSDE. Variable values of multiple linear regression models for supporting or non-supporting cases are listed in Tables 8 and 9. The coefficient of determination (R^2) for the support object used four input parameters, namely, support spacing, layer thickness,

raster angle, and inclination angle, and one output parameter, namely, the MSDE. The R^2 for the non-support object used three parameters, namely, layer thickness, raster angle, and inclination angle, and one output parameter, namely, the MSDE. The R^2s are listed in Table 10.

Table 8. Variable values of multiple linear regression models for supporting cases.

	Coefficient	Standard Error	*t*	*p*
Constant	0.08614	0.0418	2.06	0.043
Support spacing	0.022685	0.002261	10.03	**0.0**
Layer thickness	0.47917	0.05653	8.48	**0.0**
Raster angle	−0.00068	0.000251	−2.69	**0.009**
Inclination angle	−0.00584	0.000754	−7.75	**0.0**

Table 9. Variable values of multiple linear regression model for non-supporting cases.

	Coefficient	Standard Error	*t*	*p*
Constant	−0.1115	0.1275	−0.87	0.396
Layer thickness	0.3975	0.08251	4.82	**0.0**
Raster angle	−0.0006	0.000367	−1.63	0.126
Inclination angle	0.0018	0.001796	1	0.333

Table 10. The coefficient of determination (R^2) of support and non-support objects.

Object	R^2
Support	0.759
Non-support	0.659

In the case of the supporting object, the *p*-values for support spacing, layer thickness, raster angle, and inclination angle were 0.043, 0.0, 0.0, 0.009, and 0.0, respectively. The *t*-values for the support spacing, layer thickness, raster angle, and inclination angle, which had *p*-values below 0.05, were 10.03, 8.48, −2.67, and −7.75, respectively. Their standard errors were 0.00226, 0.05653, 0.000251, and 0.000754. The constant term, represented by 0.08614 of the coefficient, had a standard error of 0.0418. The *t*-value was 2.06, and the *p*-value was 0.043, indicating a statistically significant relationship. This implies that even when all predictor variables are zero, the constant term has a significant impact on the dependent variable. The MSDE, which was representative as the output, can be calculated as 0.0861 + 0.0277 × supporting space + 0.479 × layer thickness − 0.000677 × raster angle − 0.00584 × inclination angle. The R^2 between the four input parameters and one output parameter was 0.759.

In the case of the non-supporting object, the *p*-values for layer thickness, raster angle, and inclination angle were 0, 0.126, and 0.333, respectively. The *t*-values were 4.82 for layer thickness, −1.63 for raster angle, and 1 for inclination angle. Their standard errors were 0.08251, 0.000367, and 0.001796. The constant term, represented by −0.1115 of the coefficient, had a standard error of 0.1275. The *t*-value was −0.87, and the *p*-value was 0.396, indicating no statistically significant relationship. This suggests that when all other predictor variables are zero, the constant does not significantly influence the dependent variable. The MSDE was calculated as −0.111 + 0.397 × layer thickness − 0.0006 × raster angle + 0.00180 × inclination angle. The R^2 between the three parameters and one output parameter was 0.659.

In cases where support was utilized, support spacing, layer thickness, raster angle, and inclination angle were found to be statistically significant predictors of the dependent variable, as evidenced by *p*-values below 0.05. Support spacing and layer thickness exhibited positive relationships, while raster angle and inclination angle demonstrated negative relationships. In cases where support was not utilized, only layer thickness exhibited a

statistically significant influence on the dependent variable, while raster angle and inclination angle did not exhibit statistically significant relationships. These findings provide valuable insights into the factors influencing the dependent variable and can contribute to the optimization and improvement of the studied system.

3.4. ANOVA Test

In this study, the main and interaction effects of design parameters on MSDE were investigated by using the ANOVA model. The ANOVA results for supporting and non-supporting cases are listed in Tables 11 and 12. Visual representations of the main and interaction effects of design parameters for supportive cases are presented in Figures 6 and 7, respectively. Correspondingly, Figures 8 and 9 illustrate the effects on MSDE for non-supportive cases.

Table 11. ANOVA table for supporting cases.

	DOF	SS	MS	*p*
Inclination angle	2	0.42420	0.21210	0.000
Support spacing	2	0.71189	0.35594	0.000
Layer thickness	2	0.50658	0.25329	0.000
Raster angle	2	0.45701	0.22851	0.000
Inclination angle × support spacing	4	0.00517	0.00129	0.415
Inclination angle × layer thickness	4	0.00240	0.00060	0.759
Inclination angle × raster angle	4	0.00102	0.00026	0.938
support spacing × layer thickness	4	0.00540	0.00135	0.392
support spacing × raster angle	4	0.00319	0.00080	0.650
Layer thickness × raster angle	4	0.00099	0.00025	0.940
Error	48	0.06173	0.00129	
Total	80	2.17959		

Table 12. ANOVA table for non-supporting cases.

	DOF	SS	MS	*p*
Inclination angle	1	0.00328	0.00328	0.052
Layer thickness	2	0.07624	0.03812	0.001
Raster angle	2	0.04589	0.02295	0.001
Inclination angle × layer thickness	2	0.00007	0.00004	0.923
Inclination angle × raster angle	2	0.00041	0.00021	0.658
Layer thickness × raster angle	4	0.00586	0.00146	0.135
Error	4	0.00176	0.00044	
Total	17	0.13351		

The ANOVA table provides a comprehensive summary of the analysis, detailing the degrees of freedom (DOF), sum of squares (SS), mean squares (MS), and associated *p*-values for each factor, alongside the error term, as presented in Table 11. Our findings underscore the profound impact of all control parameters—namely, inclination angle, support spacing, layer thickness, and raster angle—on the output (MSDE). In Table 11, the *p*-values for all primary factors fall comfortably below the established significance threshold of 0.05, confirming their statistical significance at a confidence level of $\alpha = 0.05$. On the other hand, the interactions between these parameters showed the *p*-values were greater than 0.05, so this suggests that these interaction terms are not statistically significant and do not significantly affect the output.

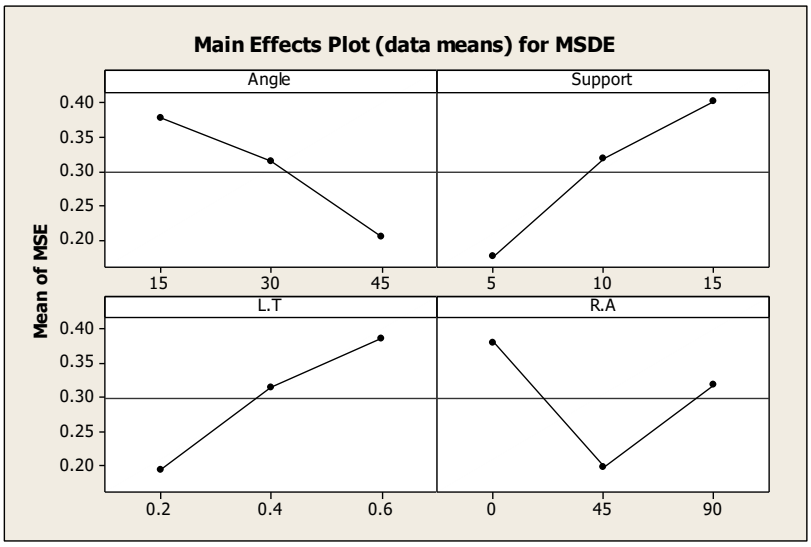

Figure 6. Main effects plot for supporting cases.

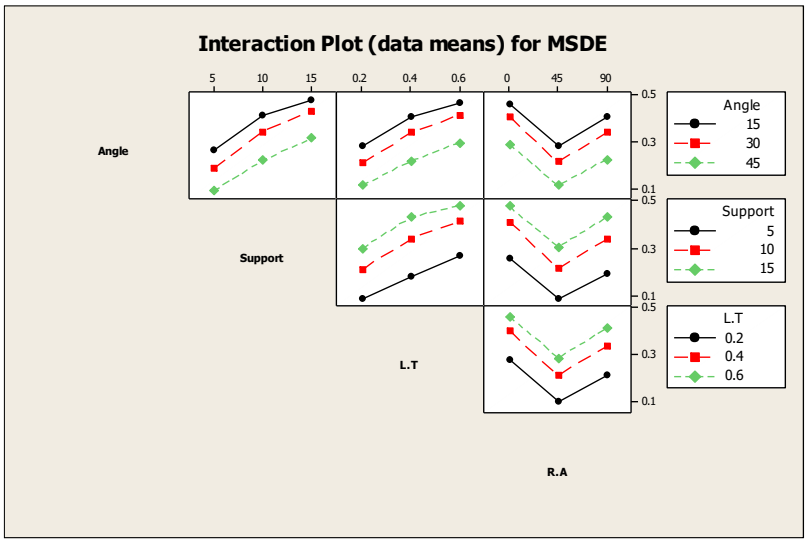

Figure 7. Interaction plot for supporting cases.

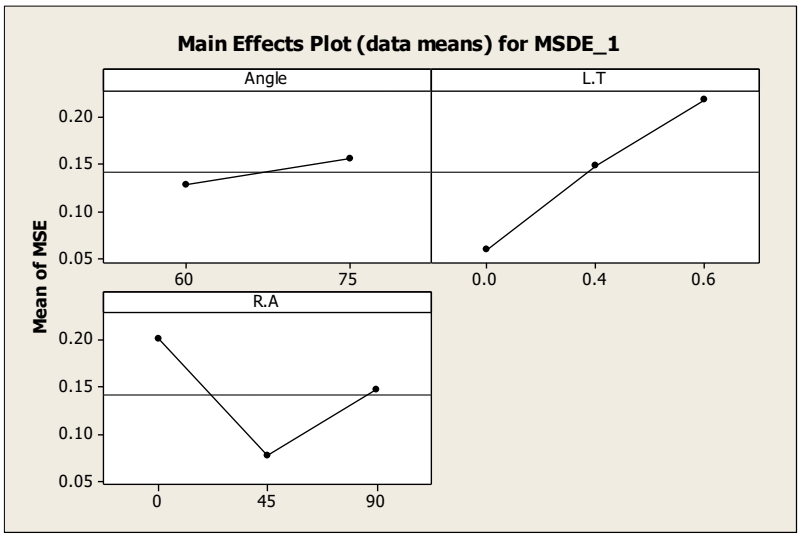

Figure 8. Main effects plot for non-supporting cases.

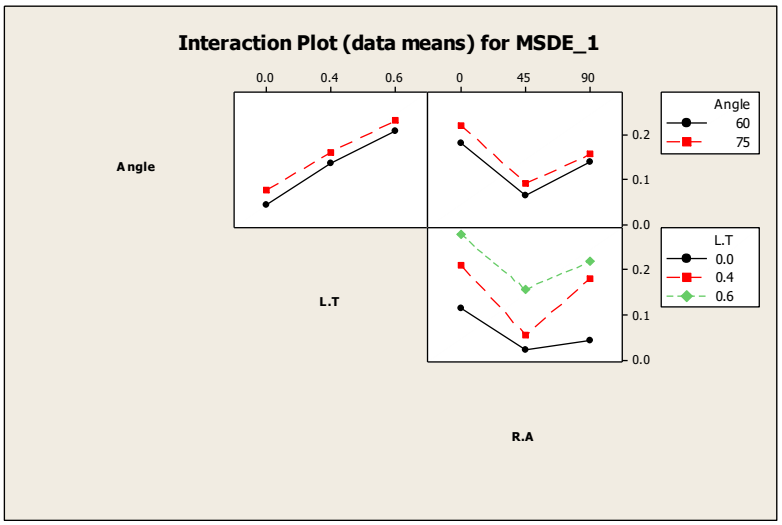

Figure 9. Interaction plot for non-supporting cases.

As illustrated in Figure 6, an increase in the inclination angle (Angle) led to a reduction in MSDE. Adjusting the inclination angle from 15° to 30° and from 30° to 45° resulted in MSDE reductions of 16.88% and 35.32%, respectively. Conversely, an increase in support spacing (Support) and layer thickness (L.T) was associated with an increase in MSDE. Specifically, increasing support spacing from 5 mm to 10 mm and from 10 mm to 15 mm led to MSDE increases of 82.31% and 25.81%, respectively. Similarly, elevating layer thickness from 0.2 mm to 0.4 mm and from 0.4 mm to 0.6 mm resulted in MSDE increases of 61.56% and 22.68%, respectively. The MSDE exhibited a declining trend with rising raster angle (R.A) until 45°, beyond which an increase was observed. Notably, the lowest MSDE was observed at a raster angle of 45°. Based on the main effect analysis, the optimal combination entailed an inclination angle of 45°, support spacing of 5 mm, layer thickness of 0.2 mm, and a raster angle of 45°. As depicted in Figure 7, the analysis indicated no significant interactions between parameters.

Table 12 presents the ANOVA results for non-supporting cases, outlining the statistical significance of main and interaction effects. Layer thickness and raster angle both exhibited significant effects on MSDE, with *p*-values smaller than 0.05. The *p*-value for the inclination angle was relatively close to the 0.05 threshold, suggesting a comparatively moderate level of significance. Regarding interactions, all terms had *p*-values exceeding 0.05.

Figure 8 depicts how an increase in inclination angle and layer thickness contributed to the MSDE increase. For instance, increasing the inclination angle from 60° to 75° led to a 20.98% MSDE increase. Similarly, augmenting layer thickness from 0 mm to 0.4 mm and from 0.4 mm to 0.6 mm resulted in MSDE increases of 150.93% and 46.71%, respectively. The MSDE followed a decreasing trend until a raster angle of 45°, beyond which it increased. Specifically, adjusting the raster angle from 0° to 45° resulted in a 61.33% MSDE reduction, followed by an 89.59% MSDE increase upon further adjustment to 90°. Based on the main effect analysis, the optimal combination consisted of a 60° inclination angle, 0.2 mm layer thickness, and a 45° raster angle. Figure 9 highlighted interaction effects, though no significant interactions were observed.

3.5. Machine Learning Regression Model Analysis

Machine learning regression models were developed to predict dimensional accuracy in this study. The calculated MAEs (errors between the measured MSDEs and the predicted MSDEs) for GPR and SVM are listed in Table 13. The R^2 between input parameters—namely, inclination angle, support space, layer thickness, and raster angle—and output parameter—namely, MSDE—for GPR and SVM were verified as shown in Figure 10. The MAEs were 0.02047 mm for GPR and 0.03476 mm for SVM, and the R^2 between the four input parameters and one output parameter for GPR and SVM were

0.98 and 0.93, respectively. Despite the utilization of a limited number of datapoints (81 datapoints), the regression models exhibited R^2 values exceeding 90%, indicating high accuracy. Compared to the recently research [29], R^2 values for GPR and SVM were higher: 12.99–18.58% or 3.23–10.00% higher than their study, respectively. Furthermore, it can be inferred that increasing the number of datapoints would lead to higher accuracies in the regression models.

Table 13. Mean absolute errors (MAEs) of the GPR and SVM models.

Regression Model	MAE
GPR	0.020473
SVM	0.034762

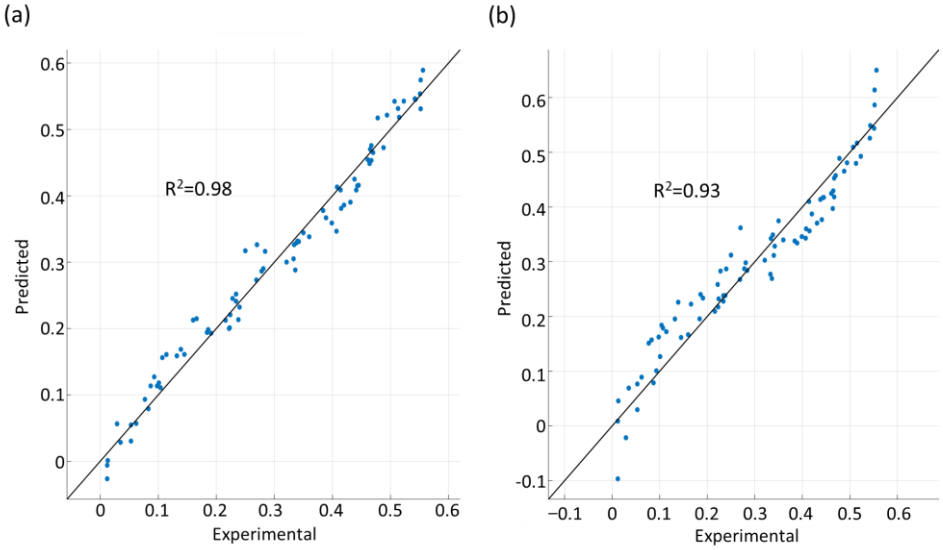

Figure 10. Prediction versus experimental plot for (**a**) GPR and (**b**) SVM regression models.

3.6. Neural Network Regression Model Analysis

In this study, the support cases (15°, 30°, and 45° of inclination angles) and non-support cases (60° and 75° of inclination angles) were trained without overfitting, as shown in Figure 11. The loss for the training dataset and the loss for the validation dataset decreased with each epoch number, and both loss datasets were converged after the 25th and 90th epoch for the MAE for support cases and the MAE for non-support cases, respectively.

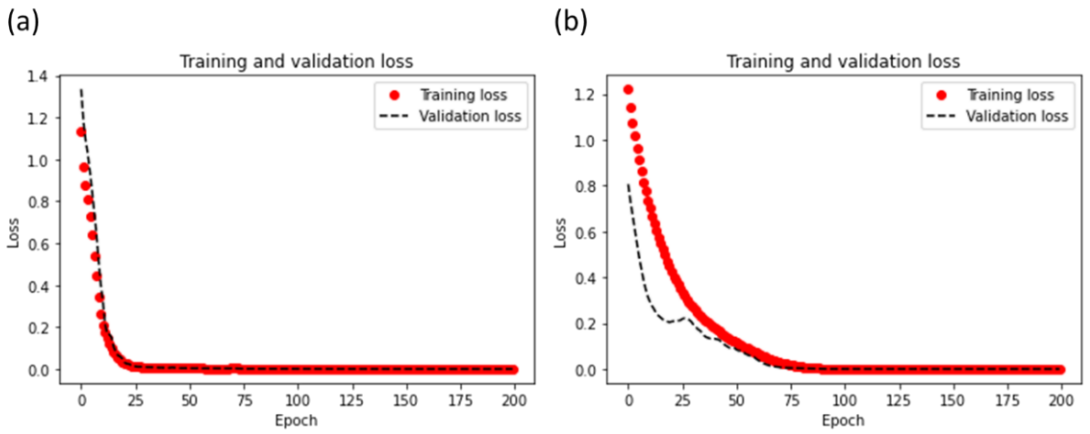

Figure 11. Training and validation losses for (**a**) support cases (15°, 30°, and 45° inclination angles) and (**b**) non-support cases (60° and 75° inclination angles).

The MAEs for the support cases were 0.0056 mm for training and 0.0055 mm for validation. The MAEs for non-support cases were 1.1172×10^{-4} mm for training and 2.1468×10^{-5} mm for validation. All MAEs are listed in Tables 14 and 15. The R^2 between the four input parameters for support cases or the three input parameters for non-support cases and one output parameter for both support and non-support cases were 0.9995 and 0.9999, respectively, as shown in Figure 12.

Table 14. Mean absolute errors (MAEs) of training and validation for the support cases.

Regression Model	MAE
Training	0.0056
Validation	0.0055

Table 15. Mean absolute errors (MAEs) of training and validation for the non-support cases.

Regression Model	MAE
Training	1.1172×10^{-4}
Validation	2.1468×10^{-5}

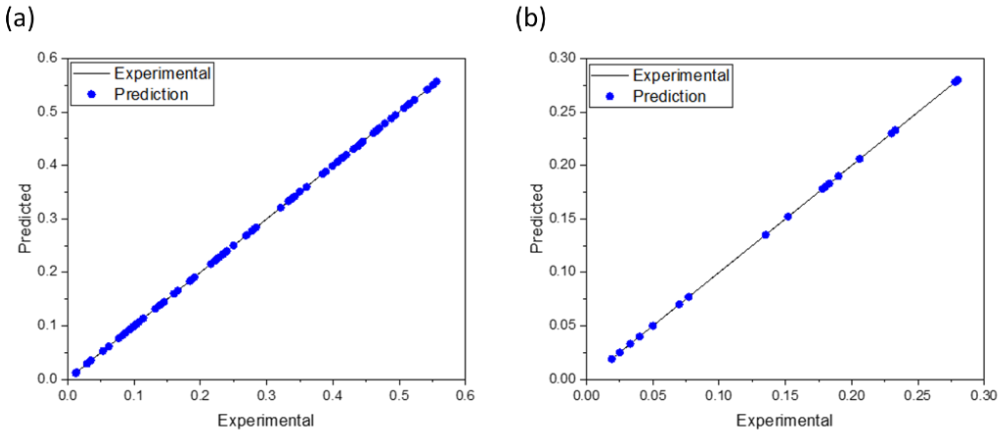

Figure 12. Prediction versus experimental plot for (**a**) support cases (15°, 30°, and 45° inclination angles) and (**b**) non-support cases (60° and 75° inclination angles).

In Figures 13–16, the effects of input parameters on the MSDE were investigated by the ANN models. In the estimation, the MSDEs were shown by varying two input variables, but other variables were fixed.

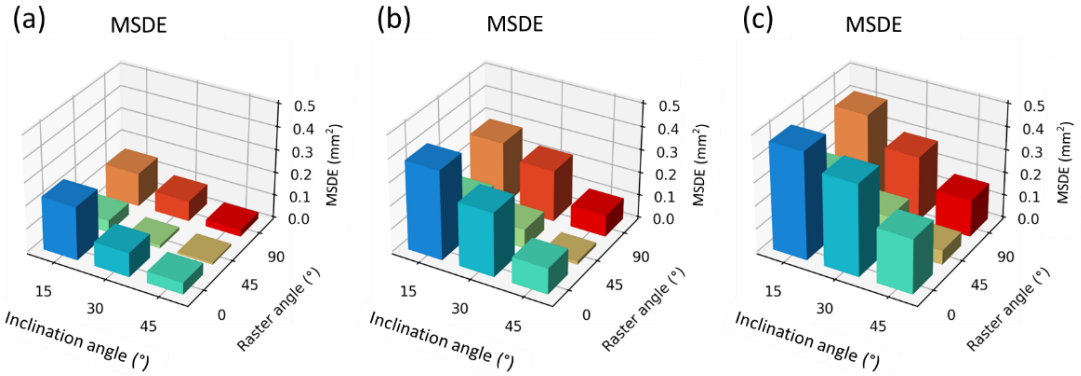

Figure 13. Predicted mean squared dimensional error (MSDE) with 5 mm of support space with layer thickness (**a**) 0.2 mm, (**b**) 0.4 mm, and (**c**) 0.6 mm.

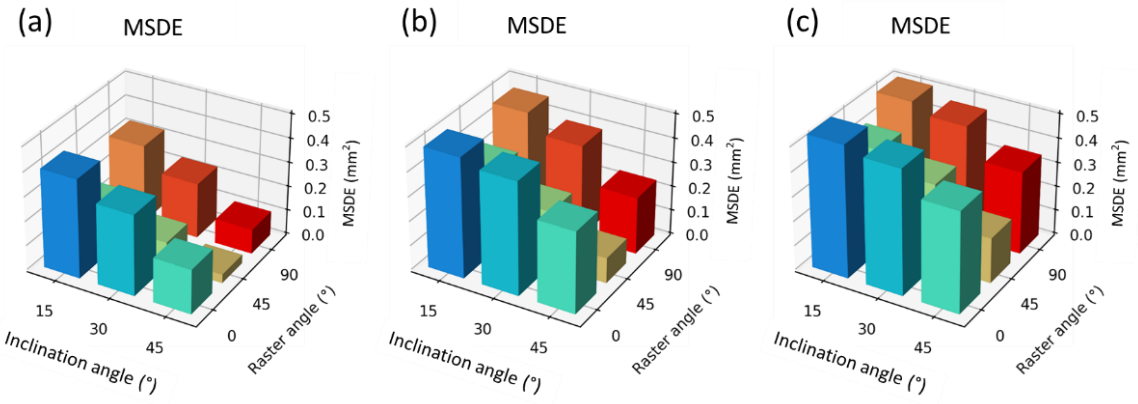

Figure 14. Predicted mean squared dimensional error (MSDE) with 10 mm of support space with layer thickness (**a**) 0.2 mm, (**b**) 0.4 mm, and (**c**) 0.6 mm.

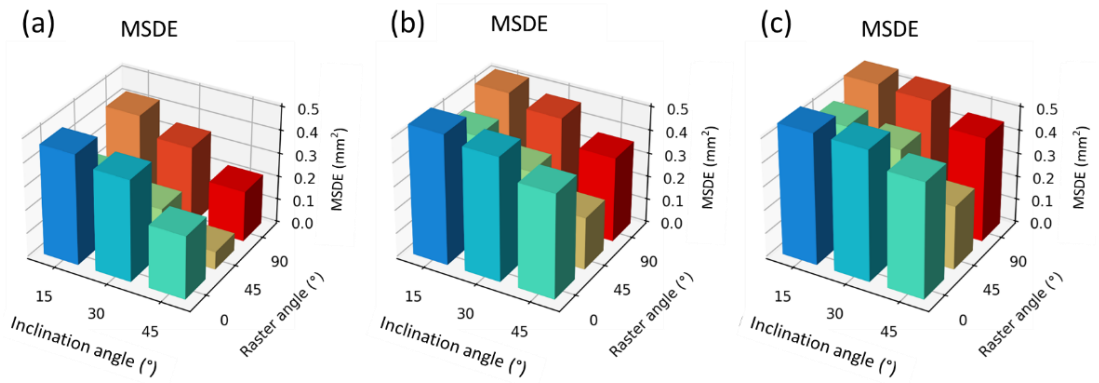

Figure 15. Predicted mean squared dimensional error (MSDE) with 15 mm of support space with layer thickness (**a**) 0.2 mm, (**b**) 0.4 mm, and (**c**) 0.6 mm.

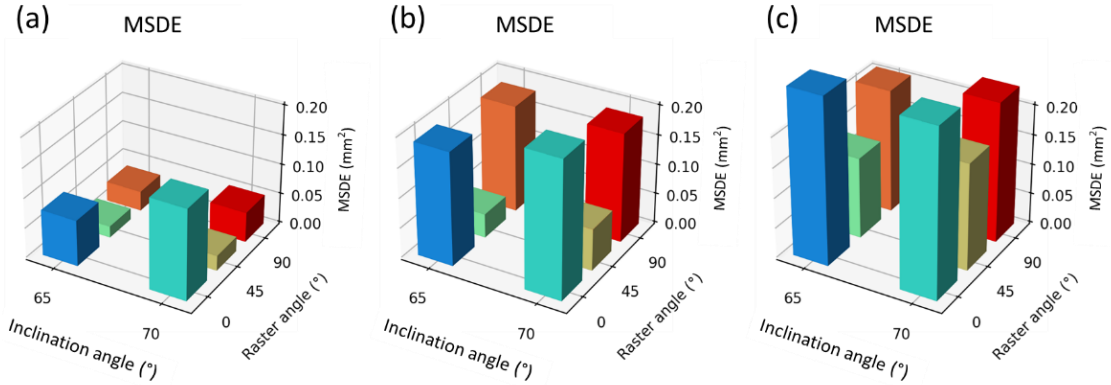

Figure 16. Predicted mean squared dimensional error (MSDE) without support space with layer thickness (**a**) 0.2 mm, (**b**) 0.4 mm, and (**c**) 0.6 mm.

Figures 13–15 present the MSDEs observed for different support space widths (5 mm, 10 mm, and 15 mm) and layer thicknesses (0.2 mm, 0.4 mm, and 0.6 mm), considering the variations in inclination angle and raster angle. Figure 16, on the other hand, displays the MSDEs for cases where no support is used, with corresponding 0.2 mm, 0.4 mm, and 0.6 mm of layer thicknesses.

In the case of utilizing support objects, an increase in inclination angle was found to result in a decrease in the MSDEs. Additionally, an increase in support space was observed to lead to an increase in the MSDEs. However, under the same inclination angle conditions, when the raster angles were set to 45°, the MSDEs exhibited relatively lower

values compared to other raster angles. In the case of utilizing the non-support object, as the inclination angle increased, the MSDEs also increased. Moreover, when the raster angle was 45°, the MSDEs were observed to be lower compared to the errors associated with other raster angles.

Increasing the inclination angle with support provides better support for overhanging features and complex geometries, maintaining structural integrity and reducing deformations. By mitigating the effects of gravity, the inclination angle with support reduces material sagging, warping, or overhangs and enables more controlled and accurate material deposition, resulting in reduced MSDEs [30]. A raster angle of 45° provides a more balanced deposition pattern during the printing process. This angle allows for a balanced distribution of stresses and forces, resulting in improved layer adhesion and reduced distortion. In contrast, at extreme angles such as 0° or 90°, the deposition pattern may introduce more inherent weaknesses, leading to increased MSDEs and reduced dimensional accuracy [28,31,32].

4. Conclusions

In this study, 3D objects with various support bars and inclination angles were manufactured using the FDM process. The main effect and interaction factor were determined for the 3D-printed object quality utilizing a multiple regression model and ANOVA test. Prediction models were formulated to forecast printing accuracy through the utilization of three distinct machine learning models.

1. The influences of support spacing, layer thickness, and raster angle were founded to be statistically significant by the Pearson and *p*-value analysis, and all parameters (supporting spacing, layer thickness, raster angle, and inclination angle) were assessed to be statistically significant predictors of the dependent variable by multiple linear regression model and ANOVA analysis. The optimal combination entailed a 45° inclination angle, 5 mm of support spacing, 0.2 mm of layer thickness, and a 45° raster angle.
2. Results of the R^2 from multiple linear regression, GPR, SVM, and the neural network model (from Python) were 76%, 98%, 93%, and 99%, respectively. MAEs for GPR and SVM were 0.020 mm and 0.034 mm. MAEs for neural network models from Python were 0.0055 mm for supporting cases and 2.1468 x 10^{-5} mm for non-supporting cases.
3. The minimum MSDE was obtained at a 45° raster angle and 45° inclination angle (when 5 mm of support space with 0.2 mm of layer thickness), according to the neural network model.

The dimensional deformations of molds, which are caused by thermal deformations such as warpage and heat distortion and can occur during the rapid tooling process, can be predicted. Using machine learning models, it is possible to predict and compare dimensional deformation for various material composites.

Author Contributions: Conceptualization, K.-E.M., J.-W.J., J.S. and S.Y.; methodology, K.-E.M., J.-W.J. and J.S.; investigation, K.-E.M., J.-W.J. and C.K.; writing—original draft preparation, K.-E.M. and C.K.; writing—review and editing, C.K. and S.Y.; project administration, J.S. and S.Y. All authors have read and agreed to the published version of the manuscript.

Funding: This study was conducted with the support of the Korea Institute of Industrial Technology as "Development of root technology for multi-product flexible production (KITECH EO-23-0008)".

Institutional Review Board Statement: Not applicable.

Informed Consent Statement: Not applicable.

Data Availability Statement: The data presented in this study are available on request from the corresponding author.

Conflicts of Interest: The authors declare no conflict of interest.

References

1. Siacor, F.D.C.; Chen, Q.; Zhao, J.Y.; Han, L.; Valino, A.D.; Taboada, E.B.; Caldona, E.B.; Advincula, R.C. On the additive manufacturing (3D printing) of viscoelastic materials and flow behavior: From composites to food manufacturing. *Addit. Manuf.* **2021**, *45*, 102043. [CrossRef]
2. Ajinjeru, C.; Kishore, V.; Liu, P.; Hassen, A.A.; Lindahl, J.; Kunc, V.; Duty, C. Rheological evaluation of high temperature polymers to identify successful extrusion parameters. In *International Solid Freeform Fabrication Symposium*; University of Texas at Austin: Austin, TX, USA, 2017.
3. Pelayo, F.; Blanco, D.; Fernandez, P.; Gonzalez, J.; Beltran, N. Viscoelastic Behaviour of Flexible Thermoplastic Polyurethane Additively Manufactured Parts: Influence of Inner-Structure Design Factors. *Polymers* **2021**, *13*, 2365. [CrossRef] [PubMed]
4. Tan, L.J.; Zhu, W.; Zhou, K. Recent progress on polymer materials for additive manufacturing. *Adv. Funct. Mater.* **2020**, *30*, 2003062. [CrossRef]
5. Ligon, S.C.; Liska, R.; Stampfl, J.; Gurr, M.; Mulhaupt, R. Polymers for 3D printing and customized additive manufacturing. *Chem. Rev.* **2017**, *117*, 10212–10290. [CrossRef] [PubMed]
6. Jang, J.-W.; Min, K.-E.; Kim, C.; Shin, J.; Lee, J.; Yi, S. Scaffold characteristics, fabrication methods, and biomaterials for the bone tissue engineering. *Int. J. Precis. Eng. Manuf.* **2023**, *24*, 511–529. [CrossRef]
7. Bourell, D.; Kruth, J.P.; Leu, M.; Levy, G.; Rosen, D.; Beese, A.M.; Clare, A. Materials for additive manufacturing. *CIRP Ann.* **2017**, *66*, 659–681. [CrossRef]
8. Ngo, T.D.; Kashani, A.; Imbalzano, G.; Nguyen, K.T.; Hui, D. Additive manufacturing (3D printing): A review of materials, methods, applications and challenges. *Compos. Part B Eng.* **2018**, *143*, 172–196. [CrossRef]
9. Kim, H.-S.; Lee, D.-Y.; Park, J.-H.; Kim, J.-H.; Hwang, J.-H.; Jung, H.-I. Optimization of electrohydrodynamic writing technique to print collagen. *Exp. Technol.* **2007**, *31*, 15–19. [CrossRef]
10. Chung, H.; Das, S. Processing and properties of glass bead particulate-filled functionally graded Nylon-11 composites produced by selective laser sintering. *Mater. Sci. Eng. A* **2006**, *437*, 226–234. [CrossRef]
11. Chung, H.; Das, S. Functionally graded Nylon-11/silica nanocomposites produced by selective laser sintering. *Mater. Sci. Eng. A* **2008**, *487*, 251–257. [CrossRef]
12. Eshraghi, S.; Das, S. Mechanical and microstructural properties of polycaprolactone scaffolds with one-dimensional, two-dimensional, and three-dimensional orthogonally oriented porous architectures produced by selective laser sintering. *Acta Biomater.* **2010**, *6*, 2467–2476. [CrossRef] [PubMed]
13. Kim, M.-S.; Chu, W.-S.; Kim, Y.-M.; Avila, A.P.G.; Ahn, S.-H. Direct metal printing of 3D electrical circuit using rapid prototyping. *Int. J. Precis. Eng. Manuf.* **2009**, *10*, 147–150. [CrossRef]
14. Im, Y.; Cho, B.; Seo, S.; Son, J.; Chung, S.; Jeong, H. Functional prototype development of multi-layer board (MLB) using rapid prototyping technology. *J. Mater. Process. Technol.* **2007**, *187*, 619–622. [CrossRef]
15. Kiran, A.S.K.; Veluru, J.B.; Merum, S.; Radhamani, A.; Doble, M.; Kumar, T.S.; Ramakrishna, S. Additive manufacturing technologies: An overview of challenges and perspective of using electrospraying. *Nanocomposites* **2018**, *4*, 190–214. [CrossRef]
16. Huang, Y.; Leu, M.C.; Mazumder, J.; Donmez, A. Additive manufacturing: Current state, future potential, gaps and needs, and recommendations. *J. Manuf. Sci. Eng.* **2015**, *137*, 014001. [CrossRef]
17. Lee, J.-Y.; An, J.; Chua, C.K. Fundamentals and applications of 3D printing for novel materials. *Appl. Mater. Today* **2017**, *7*, 120–133. [CrossRef]
18. Chang, D.-Y.; Huang, B.-H. Studies on profile error and extruding aperture for the RP parts using the fused deposition modeling process. *Int. J. Adv. Manuf. Technol.* **2011**, *53*, 1027–1037. [CrossRef]
19. Saqib, S.; Urbanic, J. An experimental study to determine geometric and dimensional accuracy impact factors for fused deposition modelled parts. In *Enabling Manufacturing Competitiveness and Economic Sustainability*; Springer: Berlin/Heidelberg, Germany, 2012; pp. 293–298.
20. Akbas, O.E.; Hira, O.; Hervan, S.Z.; Samankan, S.; Altinkaynak, A. Dimensional accuracy of FDM-printed polymer parts. *Rapid Prototyp. J.* **2020**, *26*, 288–298. [CrossRef]
21. Park, J.-M.; Jeon, J.; Koak, J.-Y.; Kim, S.-K.; Heo, S.-J. Dimensional accuracy and surface characteristics of 3D-printed dental casts. *J. Prosthet. Dent.* **2021**, *126*, 427–437. [CrossRef]
22. Jordan, M.I.; Mitchell, T.M. Machine learning: Trends, perspectives, and prospects. *Science* **2015**, *349*, 255–260. [CrossRef]
23. L'heureux, A.; Grolinger, K.; Elyamany, H.F.; Capretz, M.A. Machine learning with big data: Challenges and approaches. *IEEE Access* **2017**, *5*, 7776–7797. [CrossRef]
24. Morgan, D.; Jacobs, R. Opportunities and challenges for machine learning in materials science. *Annu. Rev. Mater. Res.* **2020**, *50*, 71–103. [CrossRef]
25. Khanzode, K.C.A.; Sarode, R.D. Advantages and disadvantages of artificial intelligence and machine learning: A literature review. *Int. J. Lib. Inf. Sci.* **2020**, *9*, 3.
26. Min, K.-E.; Jang, J.-W.; Kim, J.-K.; Yi, S.; Kim, C. Prediction of Curing Time/Shear Strength of Non-Conductive Adhesives Using a Neural Network Model. *Appl. Sci.* **2022**, *12*, 12150. [CrossRef]
27. Sood, A.K.; Ohdar, R.; Mahapatra, S.S. Improving dimensional accuracy of fused deposition modelling processed part using grey Taguchi method. *Mater. des.* **2009**, *30*, 4243–4252. [CrossRef]

28. Mohamed, O.A.; Masood, S.H.; Bhowmik, J.L. Modeling, analysis, and optimization of dimensional accuracy of FDM-fabricated parts using definitive screening design and deep learning feedforward artificial neural network. *Adv. Manuf.* **2021**, *9*, 115–129. [CrossRef]
29. Ali, A.; Riaz, R.D.; Malik, U.J.; Abbas, S.B.; Usman, M.; Shah, M.U.; Kim, I.-H.; Hanif, A.; Faizan, M. Machine Learning-Based Predictive Model for Tensile and Flexural Strength of 3D-Printed Concrete. *Materials* **2023**, *16*, 4149. [CrossRef] [PubMed]
30. Cheng, B.; Chou, K. Deformation evaluation of part overhang configurations in electron beam additive manufacturing. In Proceedings of the ASME 2015 International Manufacturing Science and Engineering Conference, Charlotte, NC, USA, 8–12 June 2014; p. V001T002A072.
31. Tontowi, A.; Ramdani, L.; Erdizon, R.; Baroroh, D. Optimization of 3D-printer process parameters for improving quality of polylactic acid printed part. *Int. J. Eng. Technol.* **2017**, *9*, 589–600.
32. Ayatollahi, M.R.; Nabavi-Kivi, A.; Bahrami, B.; Yahya, M.Y.; Khosravani, M.R. The influence of in-plane raster angle on tensile and fracture strengths of 3D-printed PLA specimens. *Eng. Fract. Mech.* **2020**, *237*, 107225. [CrossRef]